separations

MDPI

Article

In-Line Measurement of Extraction Process by Slug Flow and Determination of Mass Transfer Parameters

Takamichi Okamoto and Akinori Muto *

Department of Chemical Engineering, Graduate School of Engineering, Osaka Metropolitan University, Gakuencho 1-1, Sakai 599-8531, Japan
* Correspondence: amuto@omu.ac.jp

Abstract: The primary objective of this study was to pragmatically implement an extraction process using slug flow, wherein two immiscible phases, aqueous and oil, are alternatively channeled through a conduit to encourage mass exchange across the interface. To facilitate this, we introduced and empirically validated an in-line technique to precisely quantify the length of the slug and the potential extraction concentration of the two aforementioned phases. The length of the slug and its concentration were ascertained through conductivity, utilizing platinum wire as the electrode. This method consistently produced results with a maximum error margin of ±5%. Using this apparatus, we determined key mass transfer parameters, including the overall mass transfer coefficient. Notably, as the linear velocity amplified, so did the extraction rate. These findings present a significant opportunity for enhancing the efficiency of the extraction process and enabling its optimization.

Keywords: concentration of extractables; conductivity measurement method; extraction process; extraction rate; linear velocity; mass transfer parameters; in-line measurement; platinum wire electrode; slug flow

check for updates

Citation: Okamoto, T.; Muto, A. In-Line Measurement of Extraction Process by Slug Flow and Determination of Mass Transfer Parameters. *Separations* **2023**, *10*, 443. https://doi.org/10.3390/separations10080443

Academic Editor: Achille Cappiello

Received: 7 July 2023
Revised: 31 July 2023
Accepted: 3 August 2023
Published: 8 August 2023

Copyright: © 2023 by the authors. Licensee MDPI, Basel, Switzerland. This article is an open access article distributed under the terms and conditions of the Creative Commons Attribution (CC BY) license (https://creativecommons.org/licenses/by/4.0/).

1. Introduction

At present, a majority of chemicals and fine chemicals are produced through a batch processing method. This process involves feeding required raw materials into a reaction vessel and facilitating chemical reactions to yield the final compound. While this method is effective in generating complex substances, it presents certain disadvantages from the viewpoint of green and sustainable chemistry (GSC). The batch method is both energy and labor intensive, requiring extensive separation and purification of intermediates at each stage, and generates considerable waste.

Flow synthesis has attracted considerable attention as a novel alternative to the batch method. It utilizes slender tubes to facilitate the production of chemicals via contact with catalysts and other substances as the fluid traverses the tube system. Consequently, flow synthesis has been the subject of widespread research, primarily via studies utilizing microreactors. Microreactors offer several advantages, many of which are shared by flow synthesis [1,2]. Characteristics of flow synthesis include the laminar flow of liquid, allowing for precise control of the reaction time and the capability to manage and utilize unstable intermediate products. When the reaction volume is small, rapid mixing can be carried out, and variation in concentration during mixing is rare. The large surface area to reaction volume ratio enables easy temperature control, and the likelihood of reactor runaway or byproduct generation is minimal, even in swift exothermic reactions.

The notable features and benefits of flow synthesis are the simplicity and cleanliness of the process, conservation of energy and space, heightened safety, and a shortened distance between fundamental and applied research. Numerous studies have reported the advantages of continuous flow over conventional batch production [3–7]. The applications of flow synthesis extend beyond synthesis alone, including processes such as polymerization [8],

extraction, crystallization [9–11], and distillation [12]. A multitude of unit operations within conventional chemical engineering can now be performed based on flow processes. Future developments will likely see the combination of elemental technologies for these flow chemical processes, constructing new, environmentally friendly chemical processes. Both Europe and the United States have adopted microreactors and flow synthesis for national projects within pharmaceutical manufacturing, and significant results are anticipated. Such equipment has already seen practical applications [13].

In organic synthesis, it is indeed feasible to procure a desired product through a single reaction. However, complex compounds are typically synthesized by executing a series of reactions and separations. Extraction operations are commonly employed to distinguish different processes within chemical synthesis. If the extraction operation can be incorporated within a flow system, it provides a significant advantage by necessitating a shorter waiting period. To implement continuous extraction in flow chemical processes, a slug flow, where aqueous and oil phases alternately traverse a narrow tube, is ideally suited for extraction within flow synthesis. The use of liquid–liquid slug flow for extraction operations has been the subject of numerous past studies. Many of these studies, carried out either experimentally or by simulation, have considered conditions under which slug flow is likely to occur [13–20]. Approaches for generating slug flows [21–23], as well as the development of devices to control the slug flow shape [24], have also been thoroughly investigated. The extraction rate, or the mass transfer rate, in a slug flow depends on the shape of the slug, namely the lengths of the water and oil phases. A secondary flow, induced by twisting the flow path in a liquid–liquid slug flow, has been shown to enhance the extraction rate [25–27].

Alongside the scientific examination of slug flows, there has been substantial applied research activity, particularly in the retrieval of metal ions [28–32]. Some studies have even considered replacing conventional chemical processes. The creation of new processes, including oil–water separation [32,33] and recycling of slug streams, has been reported [34–42] based on theoretical studies. This suggests that the impact of variations in the slug flow condition on the extraction rate needs investigation. Therefore, it is crucial to ascertain the state of the slug flow within the channel.

Our objective was to continually monitor the slug flow condition over time in order to observe the process and ensure stable operation. A pressure sensor has been suggested as a method for monitoring blockages in a tube [43], although it falls short in detecting changes in the slug shape or identifying any anomalies. Monitoring of the slug flow can be achieved using an optical sensor [39], a non-intrusive method that allows for the inspection of the slug flow within the tube. However, this method presents some complexity, as it necessitates the projection of light into the tube and a window for light transmission and reception. Additionally, the light transmission through the window might be reduced due to the adherence or adsorption of certain components of the liquid flowing in the tube, hindering the swift or gradual acquisition of accurate information.

In an effort to monitor slug flow, this study sought to measure the alteration in electrical conductivity in real time. A slim metal needle electrode, posing negligible impact on the flow, was inserted externally into the flow channel, and the electrical resistance was gauged by applying a weak alternating current. This mild current did not interfere with the substances within the flow, thereby permitting an accurate determination of the flow state. A differential in conductivity was observed between the aqueous and oil phases, and the length of the slug was estimated based on the periodic fluctuations in this differential. As the extraction process progressed, the conductivity of the aqueous phase altered, and parameters related to the extraction rate were calculated from the time-dependent variation of the extraction rate.

The overall mass transfer coefficient serves as a crucial parameter for assessing extraction rate and equipment design in scientific studies involving slug flow. Numerous studies on extraction systems utilizing slug flow have highlighted its significance [44–48]. The methodology employed in this study can significantly contribute to the evaluation of

the mass transfer capacity factor. Additionally, there is a notable trend of rapid progress in the study of liquid–gas slug flow, and its application is steadily increasing, particularly in flow synthesis. High-throughput techniques, such as shortened reaction times and temperature control, have significantly contributed to advancing research on liquid–gas slug flows, both in exploration time and practical application. Although this study focuses on liquid–liquid slug flow, its results can be applied as a method to rapidly measure the length of each segment using conductivity, further enhancing the effectiveness of high-throughput techniques and serving as a technique to detect the concentration of reactants [49].

2. Experiments

2.1. Reagents

The oil phase was formulated from potassium tert-amyl oxide (25% *w*/*w* in toluene) and tris (2-ethylhexyl) phosphate (D2EHPA, Practical Grade) dissolved in cyclohexane (special grade). A solution of specified concentration was utilized. For the aqueous phase, lithium chloride (reagent, special grade) was dissolved in pure water to prepare a solution of a predetermined concentration. The respective solution concentrations are tabulated in Table 1. All the reagents were procured from FUJIFILM Wako Pure Chemical Corporation (Osaka, Japan) and were used without additional purification. Given that all compounds are highly soluble in water or exhibit solubility within the experimental parameters, they are considered to be fully ionized. This makes them well suited for concentration measurement by electric conductivity.

Table 1. Aqueous and organic solutions used in this experiment.

No.	Aqueous Solution	Organic Solution
1	Pure water	Potassium tert-pentyl oxide, 25% *w*/*w* in toluene
2	0.01 M LiCl aqueous solution	0.2 M D2EHPA cyclohexane solution
3	0.10 M LiCl aqueous solution	0.2 M D2EHPA cyclohexane solution
4	0.01 M LiCl aqueous solution	0.2 M D2EHPA cyclohexane solution
5	0.001 M LiCl aqueous solution	0.2 M D2EHPA cyclohexane solution

D2EHPA; Tris(2-ethylhexyl) Phosphate.

2.2. Experimental Apparatus and Operation

Figure 1 illustrates a schematic of the experimental apparatus used in this study. The aqueous and oil phases were fed into the system using a piezo micropump (PMP, APP-20 KG, Takasago Electric Industry Co., Ltd., Nagoya, Aichi, Japan), which offered minimal pulsation, and these phases were combined in a T-tube. Post-merging within the T-tube, a pair of platinum wires, each 0.5 mm in diameter, were inserted perpendicularly to the axial direction of the PTFE tube. The PTFE tube has an inner diameter of 0.5 mm. The platinum wire was affixed to the outside of the tube using a small amount of adhesive after creating a small hole through which the platinum wire passed, slightly protruding through the inner wall from the outside. This ensured that the platinum wire was in contact with the liquid. Only 0.1 mm of the wires came into contact with the fluid flowing within the tube. Lead wires were utilized as electrodes, connecting the platinum wires to an electrochemical measuring device (Seyssinet-Pariset, France, Bio-Logic Science Instruments, SP-150). The minimum sampling interval for this device is 2.00×10^3 μs, adequate to capture temporal variations in the slug flow. The electrochemical measurements were conducted under the following conditions: a voltage of 0.5 V, a frequency of 1 kHz, and a maximum current of 10 mA. Although the viscosity of the liquid can be influenced by the magnitude of the electric field, the experiment was designed such that the electrolysis's magnitude was not expected to impact the current value, given that measurements were made at a constant voltage, ensuring appropriate current flow in each solution. The experiment measured conductivity in a constant voltage mode. The impedance of the electrochemical apparatus is 1 TΩ, and the impedance between electrodes is sufficiently small (below 30 GHz) to not interfere with the measurements. Temporal shifts in conductivity were continuously

monitored, and data were analyzed using a personal computer. The lengths of the aqueous and oil phases of the slug flow were gauged by photographing the fluid as it coursed through the PTFE tube and determining the slug length from the captured image. Thirty images were analyzed, and the arithmetic means and standard deviations were computed. Fluid ejected from the tube was collected in a graduated cylinder for a fixed period, allowing the calculation of the volumetric flow rate from the fluid's volume. The extraction rate was determined by analyzing the concentration of each ion in the aqueous phase, which was ascertained through atomic absorption spectrophotometry (AA6200, Kyoto, Japan, SHIMADZU CORPORATION).

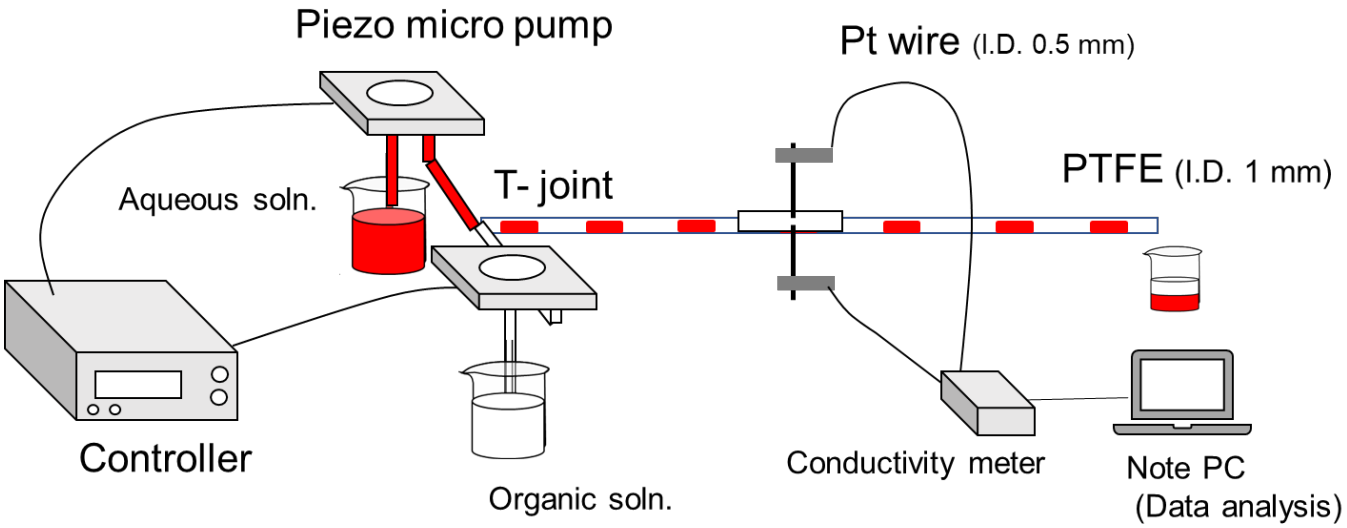

Figure 1. Experimental setup.

3. Results and Discussion

3.1. Calculation of Slug Length Based on the Difference between the Aqueous Phase, Oil Phase, and Conductivity

Organic solvents are incompatible with this process, and pure water, though possessing negligible conductivity, does exhibit minor conductivity due to the dissolved carbon dioxide in the air. By utilizing this variation in conductivity, the lengths of the aqueous and oil phases in the slug flow were determined. Figure 2 illustrates the computation of the slug length predicated on the change in conductivity.

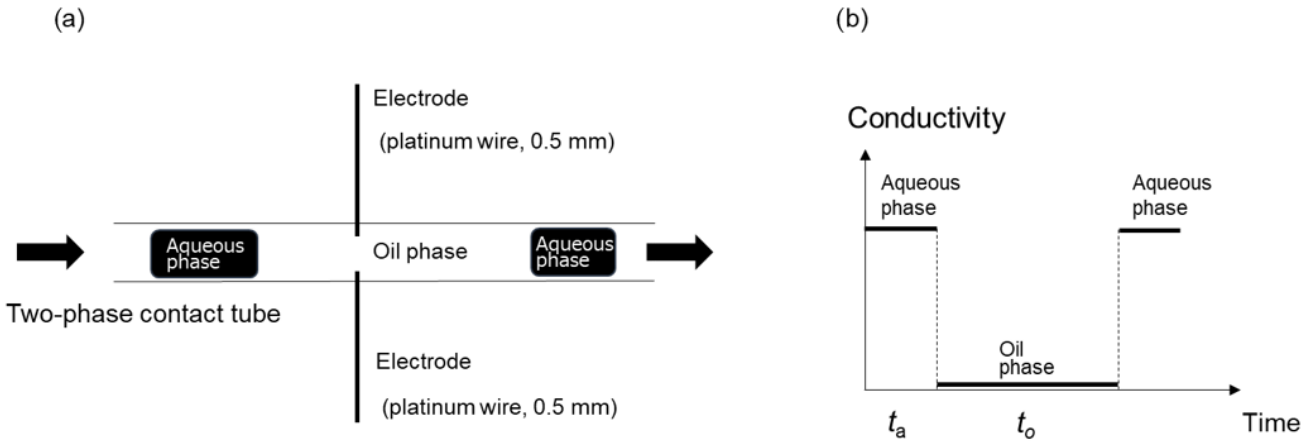

Figure 2. Image of measurement of slug length based on the change in conductivity. (**a**) Schematic diagram of a device for measuring the conductivity of a slug flow, (**b**) Time-conductivity diagram expected using the device in (**a**).

As depicted in Figure 2a, a thin platinum wire is inserted midway through the PTFE tube, through which the slug flow moves. This wire serves as an electrode for continuous measurement of conductivity. As presented in Figure 2b, a high conductivity is obtained when the water phase passes between the electrodes (t_a), and a low conductivity is recorded when the oil phase passes (t_o). The lengths of the water and oil phases of the slug flow, L_a and L_o, respectively, can be calculated by multiplying the time, t_a, which is determined from the linear velocity, u, as follows:

$$L_a = t_a \times u \quad (1)$$

$$L_o = t_o \times u \quad (2)$$

Figure 3 shows that the slug length calculated from the conductivity data closely matches the measured values obtained from the image analysis for both the water phase and the oil phase. This indicates that the conductivity response of the system is adequately sensitive for monitoring the slug flow behavior. It should be noted that at liquid linear velocities exceeding 5 cm/s (2.4 cm^3/s), the resultant aqueous- and oil-phase slug lengths are unstable, making this method unsuitable for length monitoring.

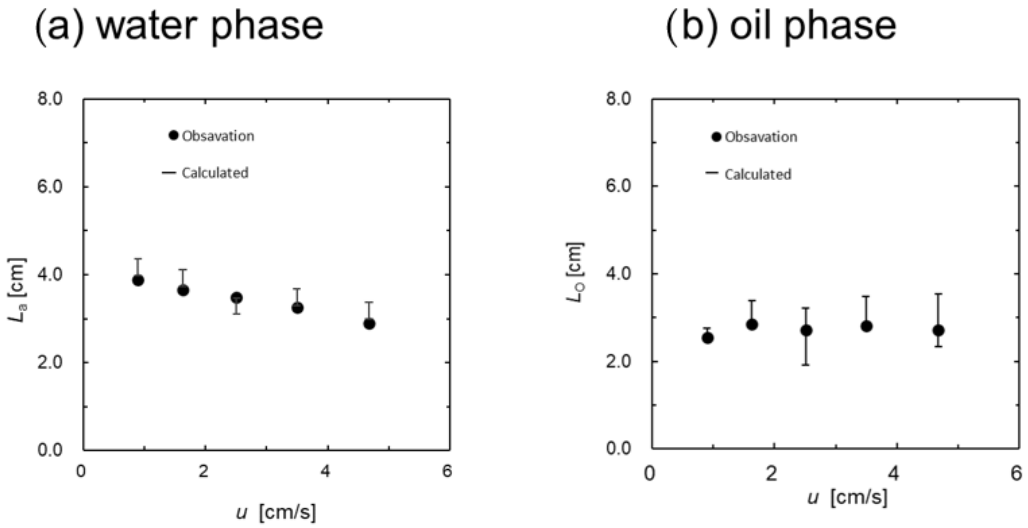

Figure 3. Comparison of slug length calculated from the electrical conductivity and the actual measurement. Flow velocity u [cm/s] (0–6) corresponds to flow volume [cm^3/s] (0–2.83). (**a**) water phase, (**b**) oil phase.

3.2. Calculation of Summary Material Capacity Factor Based on Conductivity Measurements

3.2.1. Calibration Curves for Extractability and Conductivity

For the extraction systems outlined in Table 1, solutions with various extraction rates were prepared by conducting batch experiments. The aqueous phase was then introduced into an extraction tube, and the conductivity was measured and found to be unaffected by the flow rate. The relationship between the extraction rate and conductivity for each extraction system is presented in Figure 4.

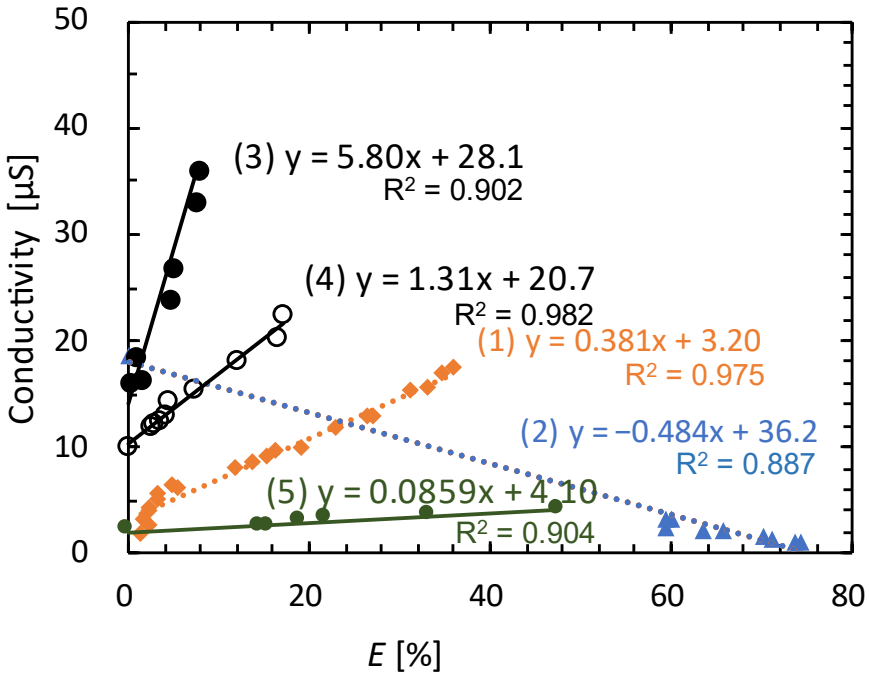

Figure 4. Relationship between the extraction rate and conductivity for each extraction system shown in Table 1.

In the hydrolysis system (System 1), the alkoxide comes into contact with water at the oil–water interface, resulting in hydrolysis that yields KOH and amyl alcohol. As KOH dissolves in the aqueous phase, conductivity increases as the extraction progresses, resulting in an almost linear calibration curve within the experimental range (extraction rate > 5%). In System 2, LiOH, which is dissolved in the aqueous phase, interacts at the oil–water interface.

$$Li^+ + OH^- + D2EHP\text{-}H^+ \rightarrow D2EHP\text{-}Li + H_2O$$

The lithium ions dissolved in the aqueous phase form complexes with D2EAPA (D2EHP-H^+), enabling them to migrate to the oil phase. Simultaneously, the OH^- ions are neutralized in water and thereby removed. Essentially, the concentration of LiOH in the aqueous phase diminishes as the extraction progresses. Due to the exceedingly high rate of this reaction, it proves challenging to prepare a solution with a low extraction rate. However, an almost linear calibration curve is still obtainable.

Systems 3–5 involve reactions between D2EHPA, dissolved in the oil phase, and lithium ions in the aqueous phase.

$$Li^+ + Cl^- + D2EHP\text{-}H^+ \rightarrow D2EHP\text{-}Li + H^+ + Cl^-$$

As the extraction proceeds, the quantity of lithium ions decreases, while the count of hydrogen ions increases in the aqueous phase.

As the conductivity of hydrogen ions exceeds that of lithium ions, the overall conductivity increases as the extraction progresses. A linear relationship was observed across all concentrations. Having been able to elucidate the calibration curve, we were able to ascertain the extraction rate from the conductivity using this relationship.

3.2.2. Comparison of Conventional and Conductivity Methods

In this experiment, aqueous- and oil-phase solutions were fed at a pre-determined flow rate, and the extraction rate's temporal alteration was assessed utilizing the apparatus depicted in Figure 1. The extraction time (τ) corresponds to the duration from the point at

which the aqueous and oil phases intersect until the moment the conductivity is measured at a specified position by a platinum electrode. The extraction time was computed by dividing the liquid's linear velocity (u) by the distance from the point of liquid confluence to the electrode (L), following the formula $\tau = L/u$. The resulting conductivity was converted to concentration using the calibration curve depicted in Figure 2, and the extraction rate was computed accordingly.

Figure 5 shows the results of conductivity measurements for the solution in System 1, operating at a flow velocity of u = 0.003 m/s. The electrodes were positioned at various points within the PTFE tube, leading to different extraction times. The ▲ symbol denotes the measurements taken using the apparatus displayed in Figure 2. Zero signifies the quantity of liquid discharged from the outlets of PTFE tubes of varying lengths. The concentration of potassium ions in the collected liquid was gauged by flame spectrometry, and the extraction rate was calculated accordingly. The quantity of potassium ions in the aqueous phase decreased as the extraction time increased, indicating ongoing extraction as the oil phase flowed through the PTFE tubes. The zero measurement was invariably larger than ▲, which can be attributed to ongoing extraction even during the brief period when the liquid discharged from the tube is in storage.

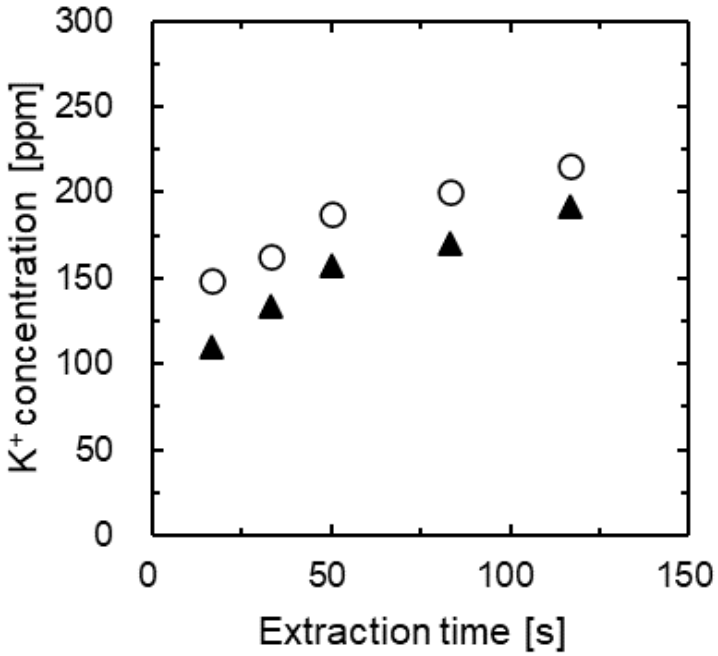

Figure 5. Comparison of concentration measurement by conductivity with conventional measurement results. In the figure, ○ represents the conventional method (Li concentration was measured using atom absorption spectrometry) and ▲ denotes the method used in this study (shown in Figure 2).

The volumetric mass transfer coefficient (K_La) serves as a parameter to assess the extraction rate and can be obtained using the following procedure [31]. At first, the mass transfer rate (N_A [mol/(L·s)]) is determined using the following equation:

$$N_A = -\frac{dC}{dt} = -K_La(C - C^*), \quad (3)$$

where t is the extraction time [s] and C^* is the Li^+ concentration [M] in the aqueous phase at extraction equilibrium. The integration of Equation (3) provides

$$-\ln(C - C^*) = K_Lat + A. \quad (4)$$

The substitution of Equation (2) into Equation (4) provides

$$-\ln\left(1-\frac{E}{E^*}\right) = K_L a t + A', \tag{5}$$

where E^* is the extraction efficiencies at equilibrium.

$$E^* = \frac{C_0 - C^*}{C_0}. \tag{6}$$

A and A' represent constants, while C_0 is the feed concentration. Equation (5) suggests that $-\ln(1 - E/E^*)$ is a linear function of extraction time t. Hence, experimental data for extraction efficiency and extraction time were employed to plot $-\ln(1 - E/E^*)$ against t. The gradient of the linear plot yielded the value of $K_L a$.

The results outlined in Figure 5 have been systematically restructured as per Equation (5) to produce Figure 6. Both exhibit a strong linear relationship, and the mass transfer coefficient ($K_L a$) was calculated from their respective slopes. The $K_L a$ value determined from conductivity was 0.0012 1/s, closely paralleling the $K_L a$ of 0.0011 1/s, which was computed through the traditional method of storing the discharged liquid. These findings suggest that determining $K_L a$ from conductivity is also an effective approach.

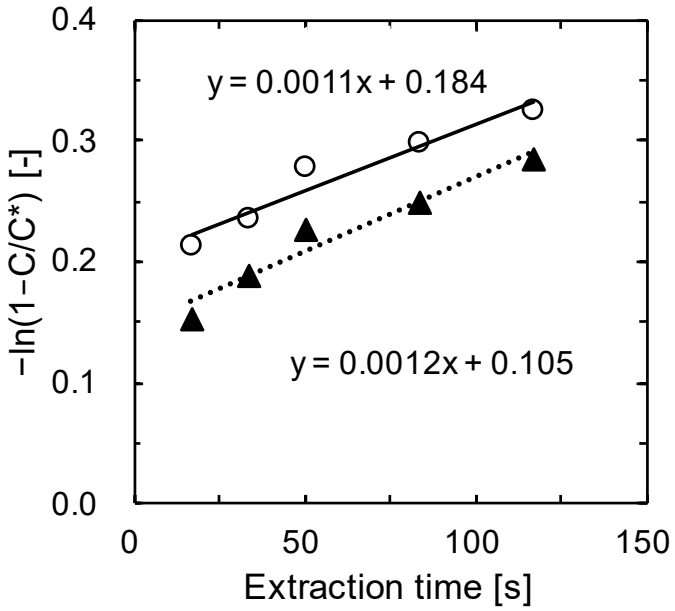

Figure 6. Overall mass transfer capacitance coefficient. In the figure, ○ represents the conventional method (Li concentration was measured using atom absorption spectrometry) and ▲ represents the method used in this study (shown in Figure 2).

3.2.3. Calculation of Specific Interfacial Area of the Oil–Water Interface of Slug Flow in a PTFE Tube

The methodology for calculating the specific interfacial area of the oil–water interface in slug flow is illustrated in Figure 7. When slug flow transits through a hydrophobic tube-like PTFE, the oil phase (cyclohexane) forms a continuous phase, and the aqueous phase transforms into a dispersed phase. Although the oil–water interface exhibits curvature, it is presumed flat, as depicted in Figure 7. The error arising from this presumption is considered to be minimal and insignificant in comparison with the overall specific interfacial area. The tube's radius is symbolized by r, while the lengths of the slugs in the oil and water phases are represented by L_o and L_a, respectively. The distance between the dispersed phase and the tube wall is considerably smaller than the tube diameter, and it is considered negligible

in terms of volume. Consequently, we determined the specific surface area per unit volume of the oil phase utilizing Equation (7).

$$a = \frac{\text{Water} - \text{oil boundary area } [\text{m}^2]}{\text{Volume of one organic phase slug } [\text{m}^3]} = \frac{2\pi r^2 + 2\pi r L_a}{V\pi r^2 L_o} \quad (7)$$

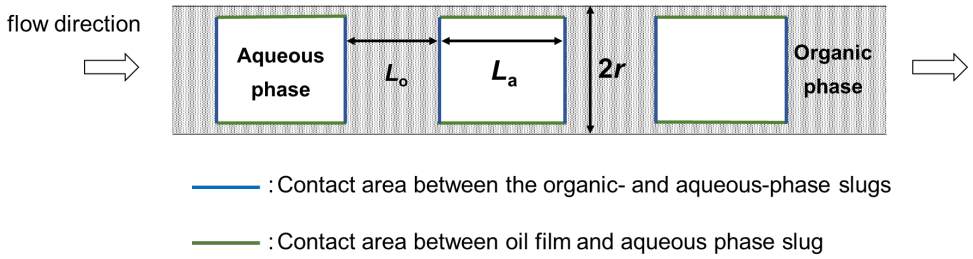

Figure 7. Calculation of specific surface area, *a*.

L_o and L_a were determined from the photographed image, and *a* was calculated using Equation (8).

3.2.4. Effect of the Linear Velocity of Liquid on Mass Transfer at the Oil–Water Interface

Experiments conducted using this apparatus allowed for the computation of the mass transfer coefficient (K_La) and mass transfer capacity coefficient (K_L) for extraction systems 1–5 (Figure 8). With this apparatus, the slug length and specific surface area remained largely constant, regardless of variations in flow velocity. Therefore, the calculated K_L reflects the impact of the liquid's linear velocity on the mass transfer rate. As the linear velocity of the liquid amplified, circulation flow within each segment of the oil and water phases intensified, thereby accelerating mass transfer and resulting in an increase in K_L. Notably, K_L was higher in Systems 1 and 2, which involved neutralization reactions, than in Systems 3–5, which did not entail such reactions.

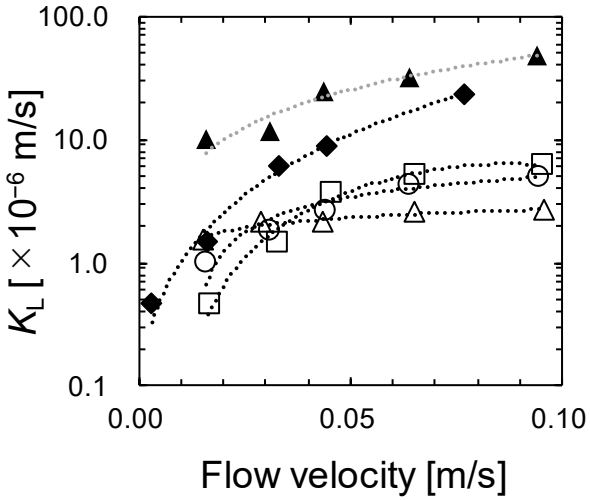

Figure 8. Effect of linear slug velocity on K_L. ▲: 1, ■: 2, □: 3, ○: 4, △: 5 The numbers are shown in Table 1. Flow velocity [cm/s] (0–0.10) corresponds to flow volume [cm^3/s] (0–0.04).

At lower liquid speeds, K_L is significantly influenced by the linear velocity. However, as the linear velocity increases, the rate of K_L's increase diminishes. In Systems 3–5, which exhibit a relatively low extraction rate absent any neutralization reaction, K_L remains nearly constant even when the linear velocity surges. This phenomenon occurs as the rise in linear velocity thins the boundary film of mass transfer at the oil–water interface, thereby

promoting mass transfer in the vicinity of the interface. Nonetheless, the reaction at the interface is rate limiting.

The concept of mass transfer in the proximity of the oil–water interface is depicted in Figure 9.

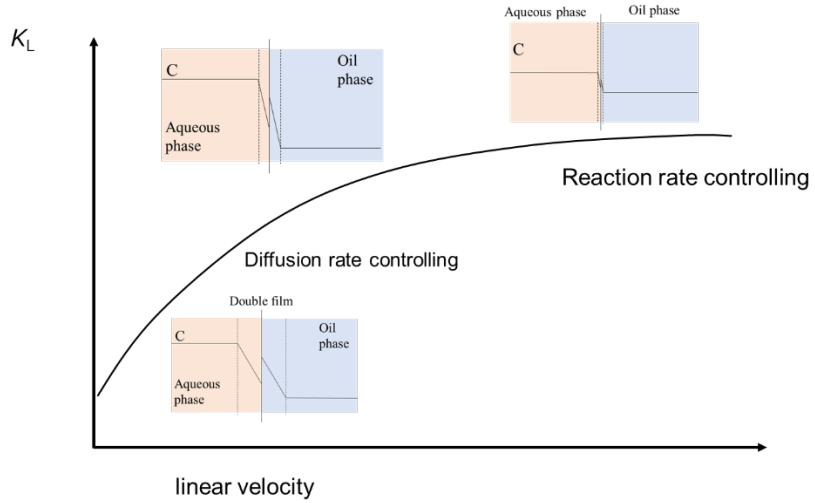

Figure 9. Conceptual diagram of mass transfer near the oil–water interface.

At lower linear velocities of the liquid, the boundary film near the interface is thick, regardless of the occurrence of circulation flow within each segment. In such a scenario, the extraction rate is controlled by the rate at which the material diffuses through the boundary film. As the linear velocity escalates, the circulation flow within each segment intensifies, and the thickness of the boundary film near the interface diminishes, which is pertinent to mass transfer. Moreover, as the linear velocity enhances, mass transfer accelerates, and the complex formation and physical dissolution reactions at the interface govern the extraction rate. This rate is recognized as the reaction rate. In this experimental setup, when the extraction rate involving the neutralization reaction is high, as observed in Systems 1 and 2, the reaction rate remains stable even if the linear flow velocity of the liquid elevates. Conversely, in systems with a relatively slow extraction rate like Systems 3–5, the apparent extraction rate stabilizes at a linear velocity of 0.05 m/s or higher, marking it as the rate-limiting reaction.

4. Conclusions

This paper proposes an extraction device and methodology predicated on the liquid–liquid slug flow approach. This method offers the benefit of calculating the slug length and extraction rate through conductivity measurement, and it allows for continuous tracking of extraction time variations over a period. The experimental outcomes derived from the extraction apparatus via the liquid–liquid slug flow method illustrate that an increase in the liquid's linear velocity bolsters mass transfer at the oil–water interface, leading to a notably higher mass transfer coefficient (K_L). In systems involving a neutralization reaction, a larger K_L was identified, compared with systems devoid of such a reaction. An extraction framework hinged on the liquid–liquid slug flow approach proves to be efficient in adjusting mass transfer effectiveness contingent on the liquid's linear velocity and the presence of a neutralization reaction.

However, it is important to acknowledge some limitations inherent in this study. It predominantly explores the effects of linear velocity, examining solely the influences of the liquid's linear velocity and the neutralization reaction on extraction efficiency. Moreover, the extraction method was tested only under constant temperature conditions. The efficacy of this extraction method warrants further testing across a broader spectrum of conditions, encompassing diverse temperatures.

In conclusion, this study imparts significant insights into the potential for extraction using the liquid–liquid slug flow method, though further research is necessary to fully comprehend its limitations. Future investigations should probe additional factors impacting the extraction efficiencies elucidated above and confirm the effectiveness of this methodology under a more extensive range of conditions.

Author Contributions: Conceptualization, A.M.; methodology, A.M.; software, A.M.; validation, T.O. and A.M.; formal analysis, T.O.; investigation, T.O.; resources, A.M.; data curation, T.O.; writing—original draft preparation, A.M. and T.O.; writing—review and editing, A.M.; visualization, T.O. and A.M.; supervision, A.M.; project administration, A.M.; funding acquisition, A.M. All authors have read and agreed to the published version of the manuscript.

Funding: This article is based on results obtained from project JPNP19004, which received funding from the New Energy and Industrial Technology Development Organization (NEDO).

Data Availability Statement: Not applicable.

Acknowledgments: This article is based on results obtained from project JPNP19004, which received funding from the New Energy and Industrial Technology Development Organization (NEDO). We would also like to thank Editage (accessed on https://cactusglobal.com/jp/, accessed on 6 July 2023) for their assistance with English language editing.

Conflicts of Interest: The authors declare no conflict of interest.

References

1. Porta, R.; Maurizio, B.; Puglisi, A. Flow Chemistry—Fundamentals Flow Chemistry: Recent Developments in the Synthesis of Pharmaceutical Products. *Org. Process Res. Dev.* **2016**, *20*, 2–25. [CrossRef]
2. Rodrigues, T.; Schneider, P.; Schneider, G. Accessing New Chemical Entities through Microfluidic Systems. *Angew. Chem. Int. Ed.* **2014**, *53*, 5750–5758. [CrossRef]
3. Taylor, C.J.; Pomberger, A.; Felton, K.C.; Grainger, R.; Barecka, M.; Chamberlain, T.W.; Bourne, R.A.; Johnson, C.N.; Lapkin, A.A. A brief introduction to chemical reaction optimization. *Chem. Rev.* **2023**, *123*, 3089–3126. [CrossRef] [PubMed]
4. Baumann, M.; Moody, T.S.; Smyth, M.; Wharry, S. A perspective on continuous flow chemistry in the pharmaceutical industry. *Org. Process Res. Dev.* **2020**, *24*, 1802–1813. [CrossRef]
5. Domokos, A.; Nagy, B.; Szilágyi, B.; Marosi, G.; Nagy, Z.K. Integrated continuous pharmaceutical technologies—A review. *Org. Process Res. Dev.* **2021**, *25*, 721–739. [CrossRef]
6. Higashio, K.; Katsuragi, S.; Kundu, D.; Adebar, N.; Plass, C.; Kühn, F.; Gröger, H.; Akai, S. Continuous-flow dynamic kinetic resolution of racemic alcohols by lipase–oxovanadium cocatalysis. *Eur. J. Org. Chem.* **2020**, *2020*, 1961–1967. [CrossRef]
7. Ahlqvist, G.P.; Burke, E.G.; Johnson, J.A.; Jamison, T.F. Continuous dimethyldioxirane generation for polymer epoxidation. *Polym. Chem.* **2021**, *12*, 489–493. [CrossRef]
8. Takahashi, Y.; Nagaki, A. Anionic Polymerization Using Flow Microreactors. *Molecules* **2019**, *24*, 1532. [CrossRef]
9. Kudo, S.; Takiyama, H. Production of Fine Organic Crystalline Particles by Using Milli Segmented Flow Crystallizer. *J. Chem. Eng. Jpn.* **2012**, *45*, 305–309. [CrossRef]
10. Furuta, M.; Mukai, K.; Cork, D.; Mae, K. Continuous crystallization using a sonicated tubular system for controlling particle size in an API manufacturing process. *Chem. Eng. Process. Process Intensif.* **2016**, *102*, 210–218. [CrossRef]
11. Hohmann, L.; Gorny, R.; Klaas, O.; Ahlert, J.; Wohlgemuth, K.; Kockmann, N. Design of a Continuous Tubular Cooling Crystallizer for Process Development on Lab-Scale. *Chem. Eng. Technol.* **2016**, *39*, 1268–1280. [CrossRef]
12. Bittorf, L.; Pathak, K.; Kockmann, N. Spinning Band Distillation Column–Rotating Element Design and Vacuum Operation. *Ind. Eng. Chem. Res.* **2021**, *60*, 10854–10862. [CrossRef]
13. Wu, H.; Khan, M.A.; Hussain, A.S. Process Control Perspective for Process Analytical Technology: Integration of Chemical Engineering Practice into Semiconductor And Pharmaceutical Industries. *Chem. Eng. Commun.* **2007**, *194*, 760–779. [CrossRef]
14. Ma, H.; Zhao, Q.; Yao, C.; Zhao, Y.; Chen, G. Effect of fluid viscosities on the liquid-liquid slug flow and pressure drop in a rectangular microreactor. *Chem. Eng. Sci.* **2021**, *241*, 116697. [CrossRef]
15. Kovalev, A.V.; Yagodnitsyna, A.A.; Bilsky, A.V. Flow hydrodynamics of immiscible liquids with low viscosity ratio in a rectangular microchannel with T-junction. *J. Chem. Eng.* **2018**, *352*, 120–132. [CrossRef]
16. Ma, D.; Liang, D.; Zhu, C.; Fu, T.; Ma, Y.; Yuan, X.; Li, H.Z. The breakup dynamics and mechanism of viscous droplets in Y-shaped microchannels. *Chem. Eng. Sci.* **2021**, *231*, 116300. [CrossRef]
17. Yi, H.; Zhu, C.; Fu, T.; Ma, Y. Interfacial evolution and dynamics of liquid bridge during droplet coalescence in rectangular microchannels: Effect of aspect ratio. *J. Taiwan Inst. Chem. Eng.* **2021**, *123*, 59–67. [CrossRef]
18. Wang, X.; Wang, Y.; Li, F.; Li, L.; Ge, X.; Zhang, S.; Qiu, T. Scale-up of microreactor: Effects of hydrodynamic diameter on liquid–liquid flow and mass transfer. *Chem. Eng. Sci.* **2020**, *226*, 115838. [CrossRef]

19. Wang, X.; Wang, K.; Riaud, A.; Wang, X.; Luo, G. Experimental study of liquid/liquid second-dispersion process in constrictive microchannels. *Chem. Eng. Sci.* **2014**, *254*, 443–451. [CrossRef]
20. Fu, G.; Chen, F.; Wei, D.; Ni, L.; Jiang, J.; Pan, Y. Hydrodynamics and mass transfer of liquid-liquid two-phase flow in circular milli-channels: Sizing-up effect. *J. Taiwan Inst. Chem. Eng.* **2022**, *141*, 104602. [CrossRef]
21. Hosseini Kakavandi, F.; Rahimi, M.; Jafari, O.; Azimi, N. Liquid–liquid two-phase mass transfer in T-type micromixers with different junctions and cylindrical pits. *Chem. Eng. Process. Process Intensif.* **2016**, *107*, 58–67. [CrossRef]
22. Sattari-Najafabadi, M.; Nasr Esfahany, M.; Wu, Z.; Sundén, B. Hydrodynamics and mass transfer in liquid-liquid non-circular microchannels: Comparison of two aspect ratios and three junction structures. *J. Chem. Eng.* **2017**, *322*, 328–338. [CrossRef]
23. Biswas, G.; Das, G.; Ray, S.; Basu, J.K. Mass transfer characteristics of liquid–liquid flow in small diameter conduits. *Chem. Eng. Sci.* **2015**, *122*, 652–661. [CrossRef]
24. Muto, A.; Abe, H.; Kanki, K.; Fukuda, T.; Kawasaki, S. Generation of controlled liquid–liquid slug flow by interlocking two diaphragm pumps. *Separations* **2022**, *9*, 97. [CrossRef]
25. Biswas, K.G.; Ray, S.; Das, G.; Basu, J.K. A simple flow device for enhanced mass transfer in reduced dimensions. *Chem. Eng. J.* **2015**, *279*, 973–982. [CrossRef]
26. Barz, D.P.J.; Zadeh, H.F.; Ehrhard, P. Laminar flow and mass transport in a twice–folded microchannel. *AIChE J.* **2008**, *54*, 381–393. [CrossRef]
27. Kurt, S.K.; Vural Gürsel, I.; Hessel, V.; Nigam, K.D.P.; Kockmann, N. Liquid–liquid extraction system with microstructured coiled flow inverter and other capillary setups for single-stage extraction applications. *Chem. Eng. J.* **2016**, *284*, 764–777. [CrossRef]
28. Hirayama, Y.; Hinoue, M.; Tokumoto, H.; Matsuoka, A.; Noishiki, K.; Muto, A. Liquid–liquid extraction and separation of cobalt and lithium ions using a slug flow microreactor. *J. Chem. Eng. Japan* **2018**, *51*, 222–228. [CrossRef]
29. Muto, A.; Hirayama, Y.; Tokumoto, H.; Matsuoka, A.; Noishiki, K. Liquid–liquid extraction of lithium ions using a slug flow microreactor: Effect of extraction reagent and microtube material, solvent extraction and ion exchange. *Solvent Extr. Ion Exch.* **2017**, *35*, 61–73. [CrossRef]
30. Sen, N.; Singh, K.K.; Mukhopadhyay, S.; Shenoy, K.T. Microfluidic extraction of uranium from dilute streams using TiAP in ionic liquid as the solvent. *Chem. Eng. Res. Des.* **2022**, *177*, 83–95. [CrossRef]
31. Kashid, M.N.; Harshe, Y.M.; Agar, D.W. Liquid–liquid slug flow in a capillary: An alternative to suspended drop or film contactors. *Ind. Eng. Chem. Res.* **2007**, *46*, 8420–8430. [CrossRef]
32. Zhou, Y.; Zhuo, C.; Huang, J.; Liu, H.; Xu, J. A microextraction approach for rapid extraction and separation of Mn(II) and Co(II) using saponified D2EHPA system. *Front. Chem. Sci. Eng.* **2021**, *16*, 963–972. [CrossRef]
33. Xu, C.; Xie, T. Review of Microfluidic Liquid–Liquid Extractors. *Ind. Eng. Chem. Res.* **2017**, *56*, 7593–7622. [CrossRef]
34. Nishiyama, Y.; Fujii, A.; Mori, H. Photoreduction synthesis of various azoxybenzenes by visible-light irradiation under continuous flow conditions. *J. Flow Chem.* **2021**, *12*, 71–77. [CrossRef]
35. Xie, T.; Ma, Y.; Xu, C. Passive continuous flow microextraction/stripping system with high throughput. *Chem. Eng. Sci.* **2020**, *223*, 115745. [CrossRef]
36. Cao, Z.; Wu, Z.; Sundén, B. Dimensionless analysis on liquid-liquid flow patterns and scaling law on slug hydrodynamics in cross-junction microchannels. *Chem. Eng. J.* **2018**, *344*, 604–615. [CrossRef]
37. Ganguli, A.A.; Pandit, A.B. Hydrodynamics of liquid-liquid flows in micro channels and its influence on transport properties: A review. *Energies* **2021**, *14*, 6066. [CrossRef]
38. Xie, T.; Liu, X.; Xu, C.; Chen, J. Intensification of liquid-liquid mass transfer by oscillation in a high-throughput microextractor. *Chem. Eng. Process. Process Intensif.* **2017**, *120*, 9–19. [CrossRef]
39. Matsuoka, A.; Mae, K. Liquid–liquid extraction performance of circulation-extraction method using a microchannel device. *Solvent Extr. Ion Exch.* **2021**, *39*, 785–805. [CrossRef]
40. Xu, B.; Cai, W.; Liu, X.; Zhang, X. Mass transfer behavior of liquid–liquid slug flow in circular cross-section microchannel. *Chem. Eng. Res. Des.* **2013**, *91*, 1203–1211. [CrossRef]
41. Al-Azzawi, M.; Mjalli, F.S.; Husain, A.; Al-Dahhan, M. A review on the hydrodynamics of the liquid–liquid two-phase flow in the microchannels. *Ind. Eng. Chem. Res.* **2021**, *60*, 5049–5075. [CrossRef]
42. Facchin, I.; Martins, J.W.; Zamora, P.G.P.; Pasquini, C. Single-phase liquid-liquid extraction in monosegmented continuous-flow systems. *Anal. Chim. Acta* **1994**, *285*, 287–292. [CrossRef]
43. Yoshiaki, T.; Tonomura, O.; Isozaki, K.; Hasebe, S. Detection and diagnosis of blockage in parallelized microreactors. *Chem. Eng. J.* **2011**, *167*, 483–489. [CrossRef]
44. Song, J.; Cheng, B.; Wang, Y.; Deng, J.; Luo, G. A microfluidic chip structure with ultra-high liquid–liquid mass transfer performance. *Sep. Purif. Technol.* **2023**, *324*, 124440. [CrossRef]
45. Karim, H.; Castel, C.; Lélias, A.; Magnaldo, A.; Sarrat, P. Kinetic study of uranium (VI) extraction with tributyl-phosphate in a stratified flow microchannel. *Sep. Purif. Technol.* **2023**, *314*, 124489. [CrossRef]
46. Ganguli, A.A.; Pandit, A.B.; Kunzru, D. Transport phenomena in microchannels in liquid–liquid extraction (LLE) systems operating in a slug flow regime—A review. *Can. J. Chem. Eng.* **2023**, 1–22. [CrossRef]
47. Zhang, D.; Cao, R.; Fu, L.; Zhang, Y. Experimental and numerical studies of separation intensification in segmented flow microreactors. *Chem. Eng. Process.* **2023**, *176*, 108905. [CrossRef]

48. Matsuoka, A.; Mae, K. Design strategy of a microchannel device for liquid–liquid extraction based on the relationship between mass transfer rate and two-phase flow pattern. *Chem. Eng. Process.* **2023**, *160*, 108297. [CrossRef]
49. Hsieh, W.H.; Coley, W.C.; Baumgartner, L.M.; Jensen, K.F.; Robinson, R.I. Photoredox Iridium−Nickel Dual-Catalyzed Decarboxylative Arylation Cross-Coupling: From Batch to Continuous Flow via Self-Optimizing Segmented Flow Reactor. *Org. Process Res. Dev.* **2018**, *22*, 542–550. [CrossRef]

Disclaimer/Publisher's Note: The statements, opinions and data contained in all publications are solely those of the individual author(s) and contributor(s) and not of MDPI and/or the editor(s). MDPI and/or the editor(s) disclaim responsibility for any injury to people or property resulting from any ideas, methods, instructions or products referred to in the content.